Brownian dynamics simulations of ions channels: A general treatment of electrostatic reaction fields for molecular pores of arbitrary geometry

Wonpil Im and Benoît Roux[a)]
Department of Biochemistry, Weill Medical College of Cornell University, New York, New York 10021

(Received 27 March 2001; accepted 18 June 2001)

A general method has been developed to include the electrostatic reaction field in Brownian dynamics (BD) simulations of ions diffusing through complex molecular channels of arbitrary geometry. Assuming that the solvent is represented as a featureless continuum dielectric medium, a multipolar basis-set expansion is developed to express the reaction field Green's function. A reaction field matrix, which provides the coupling between generalized multipoles, is calculated only once and stored before the BD simulations. The electrostatic energy and forces are calculated at each time step by updating the generalized multipole moments. The method is closely related to the generalized solvent boundary potential [Im *et al.*, J. Chem. Phys. **114**, 2924 (2001)] which was recently developed to include the influence of distant atoms on a small region part of a large macromolecular system in molecular dynamics simulations. It is shown that the basis-set expansion is accurate and computationally inexpensive for three simple models such as a spherical ionic system, an impermeable membrane system, and a cylindrical pore system as well as a realistic system such as OmpF porin with all atomic details. The influence of the static field and the reaction field on the ion distribution and conductance in the OmpF channel is studied and discussed.
 [DOI: 10.1063/1.1390507]

I. INTRODUCTION

Brownian dynamics (BD) represents an attractive computational approach for simulating the permeation process through ion channels over long time-scales without having to treat a system in all atomic details explicitly.[1–10] The approach consists in generating the chaotic trajectory of the ions as a function of time by numerically integrating stochastic equation of motions using some effective potential function to calculate the microscopic forces operating between them.[11–13] In such BD simulations, the potential function itself is a central element because it provides the underlying thermodynamic structure of the theory, i.e., it completely determines all the equilibrium properties of the system. From a microscopic point of view, this effective potential is a many-body potential of mean force (PMF) which corresponds rigorously to the reversible thermodynamic work function (free energy) to assemble a particular configuration of the ions in the system while averaging over the remaining degrees of freedom (e.g., solvent molecules, protein channel, bilayer membrane, and remote counterions).[14] Such a PMF can be calculated from molecular dynamics simulations with explicit solvent, but this is computationally intensive.[15] In the case of wide aqueous pores, a continuum electrostatic description in which the solvent is represented by a featureless dielectric medium can often be a valid and useful approximation.[16] In this context, the PMF can be expressed as a sum of various contributions including a static field arising from the fixed protein charges, and a reaction field arising from the various dielectric boundaries in the simulation system.[9,14]

Once a continuum electrostatic model is adopted, the main task consists in designing and implementing the model into a reasonably efficient computational scheme for BD simulations. Important technical difficulties are encountered, particularly in trying to incorporate the influence of the reaction field accurately. The difficulties are caused by the fact that the reaction field depends on the instantaneous configuration of the ions. In contrast, the treatment of the static field arising from the fixed protein charges is relatively simple because it can be calculated once and stored for computational efficiency. A straightforward solution might be to solve the Poisson–Boltzmann (PB) equation ''on the fly,'' at every time step during BD simulations. However, this is generally impractical because a repeated solution to the PB equation is too expensive computationally. To avoid this problem, Chung and co-workers have used an interpolation method and a large look-up table to store a discretized representation of the Green's function of the system.[6,7,10,17] The reaction field energy of a given ion configuration can be reconstructed from the stored information. A similar method was used by Coalson and co-workers.[18] To reduce the storage requirement (the Green's function depends on six spatial coordinates), applications have been limited to simplified model channels with perfect cylindrical geometry. At the present time there is no general and computationally inexpensive method for the treatment of the reaction field in a complex molecular pore of arbitrary shape. This has severely impeded the application

[a)]Electronic mail: Benoit.Roux@med.cornell.edu

of BD to realistic detailed atomic models of biological channels.

The goal of the present work is to develop a general treatment to include the influence of the electrostatic reaction field in the case of an ion channel of arbitrary geometry. The reaction field is expressed in terms of a generalized multipolar basis-set expansion of the Green's function for the system. The method is an extension to the generalized solvent boundary potential (GSBP), which has been developed to simulate a small region of a large macromolecular system.[19,20] The reaction field basis-set expansion method is incorporated into an algorithm combining Grand Canonical Monte Carlo (GCMC) and BD which was recently developed to allow for a realistic implementation of boundary conditions of ion concentration and transmembrane potential in simulations of ion channels.[9] GCMC/BD is closely related to the dual-volume-control molecular dynamics method (DVC/MD) which has been used to study diffusion problems through porous membranes.[21–24] The combined GCMC/BD algorithm with the present treatment of the reaction field using a generalized basis-set expansion provides a useful framework for simulating non-equilibrium ion fluxes through membrane channels.

In Sec. II, the GCMC/BD algorithm is briefly summarized and a microscopic model based on the continuum electrostatic approximation is presented. The formalism for the reaction field basis-set expansion method is then developed and its numerical implementation is described in detail. In Sec. III, the method is first tested and illustrated with simple model systems comprising an ionic salt solution, an impermeable membrane, and a cylindrical pore. The method is then used to simulate a detailed atomic model of OmpF porin and calculate the conductance of the channel in 200 mM KCl salt solution. The paper is concluded with a brief summary of the main results.

II. THEORETICAL DEVELOPMENTS

A. GCMC/BD algorithm

The implementation of the GCMC/BD algorithm[9] for simulating the diffusion of ions through a channel embedded in a bilayer membrane surrounded by aqueous salt solutions is schematically illustrated in Fig. 1. A spherical geometry for the simulation region is shown for convenience, though other choices are also possible. The system is divided into five specific spatial regions: the inner region, the buffer regions on sides I and II, and the outer regions on sides I and II. The Cartesian coordinates of the n_α ions of type α in the volume V are represented by $\mathbf{R}_\alpha \equiv (\mathbf{r}_\alpha^{(1)}, \mathbf{r}_\alpha^{(2)}, \ldots, \mathbf{r}_\alpha^{(n_\alpha)})$. The stochastic trajectory of all the ions in the system (inner and buffer regions) is generated with[25]

$$\dot{\mathbf{r}}_\alpha^{(i)}(t) = \frac{D_\alpha}{k_B T} \langle \mathbf{F}_\alpha^{(i)} \rangle + \zeta_\alpha^{(i)}(t), \tag{1}$$

where D_α is the diffusion constant of ions of type α, and $\zeta_\alpha^{(i)}(t)$ is a random Gaussian noise with $\langle \zeta_\alpha^{(i)}(t) \cdot \zeta_\alpha^{(j)}(0) \rangle = 6 D_\alpha \delta_{ij}(t)$. The forces acting on the ions are calculated from the gradient of the multi-ion PMF $\mathcal{W}$ of the system

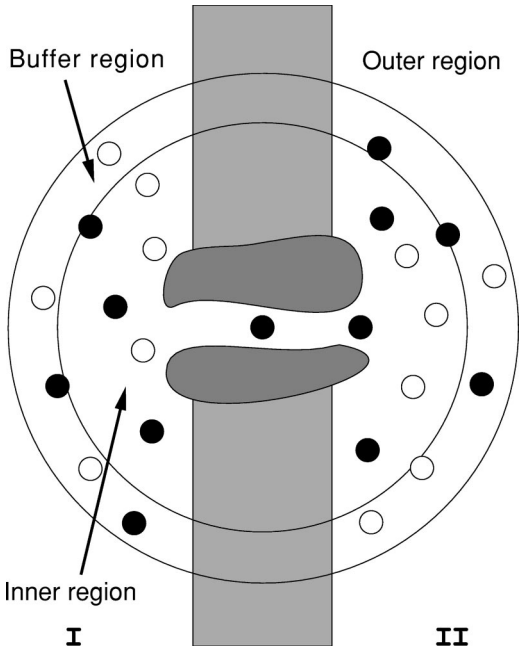

FIG. 1. Schematic representation of an ion channel-membrane system with the various regions for GCMC/BD simulations. The membrane potential is zero on the extreme left-hand side of the membrane (side I) and V_{mp} on the extreme right-hand side (side II). The channel system is divided into five specific spatial regions: the inner region, the buffer regions on sides I and II, and the outer regions on sides I and II. In the inner and buffer regions, the ions are treated explicitly and their trajectories are calculated according to BD with Eq. (1). In the buffer regions on sides I and II, the concentration of the ions are maintained in equilibrium with their corresponding bulk solution using the GCMC procedure. In the outer region the ions are treated implicitly. The electrostatic potential is calculated using the modified Poisson–Boltzmann (PB) equation given in Eq. (9).

$$\langle \mathbf{F}_\alpha^{(i)} \rangle = - \frac{\partial \mathcal{W}(n_1, n_2, \ldots; \mathbf{R}_1, \mathbf{R}_2, \ldots)}{\partial \mathbf{r}_\alpha^{(i)}}. \tag{2}$$

To ensure that external conditions are maintained on the boundaries of the inner region, the ions in the buffer regions I and II on both sides of the membrane are kept in equilibrium with the bulk solution with which they are in contact. This is enforced via the GCMC algorithm with particle creation and destruction in the two buffer regions.[9] Given that the system contains n_α ions of type α, the creation probability of an ion of that type in a randomly selected buffer region,

$$P_{\mathrm{creat}} = \frac{(\overline{n}_\alpha / (n_\alpha + 1)) \exp[-(\Delta \mathcal{W} - \overline{\mu}_\alpha)/k_B T]}{1 + (\overline{n}_\alpha / (n_\alpha + 1)) \exp[-(\Delta \mathcal{W} - \overline{\mu}_\alpha)/k_B T]}, \tag{3}$$

where $\overline{n}_\alpha$ is the expectancy for the number of ions of type α from the bulk density $\overline{\rho}_\alpha$ and the volume of the buffer region, $\overline{\mu}_\alpha$ is the chemical potential, and $\Delta \mathcal{W} \equiv [\mathcal{W}(\ldots, n_\alpha + 1, \ldots) - \mathcal{W}(\ldots, n_\alpha, \ldots)]$ is the PMF change of the system due to the new ion. The destruction probability of an ion of type α is

$$P_{\mathrm{destr}} = \frac{1}{1 + (\overline{n}_\alpha / n_\alpha) \exp[-(\Delta \mathcal{W} - \overline{\mu}_\alpha)/k_B T]}, \tag{4}$$

where $\Delta\mathcal{W}\equiv[\mathcal{W}(\ldots,n_\alpha,\ldots)-\mathcal{W}(\ldots,n_\alpha-1,\ldots)]$ is the PMF change of the system due to particle removal. The chemical potential of ions of type α in each buffer region is specified by

$$\begin{aligned}\bar{\mu}_\alpha(\mathrm{I})&=\Delta\mu_\alpha(\mathrm{I}), && \text{buffer region, side I,}\\ \bar{\mu}_\alpha(\mathrm{II})&=\Delta\mu_\alpha(\mathrm{II})+q_\alpha V_{\mathrm{mp}}, && \text{buffer region, side II,}\end{aligned} \tag{5}$$

where V_{mp} is the equilibrium electrode potential far away on side II (see Fig. 1) and $\Delta\mu_\alpha(\mathrm{I})$ and $\Delta\mu_\alpha(\mathrm{II})$ are the excess solvation energies which are influenced by ion–ion interactions in the bulk solution and are, thus, concentration dependent. The algorithm can be used to simulate equilibrium as well as nonequilibrium conditions of ion diffusion and permeation.[9]

The multi-ion PMF takes into account the interactions between all the ions present in the simulation region and the influence of the channel, the transmembrane potential, as well as implicit salt in the outer region. For the sake of simplicity, we choose to represent the solvent as a structureless dielectric medium and incorporate its influence implicitly. A rigorous rational for this type of approximation is provided by the MacMillan–Mayer theory of ionic solutions.[26] It follows that the multi-ion PMF is

$$\begin{aligned}&\mathcal{W}(\mathbf{R}_1,\mathbf{R}_2,\ldots)\\ &=\sum_{\alpha\gamma}\sum_{ij}u_{\alpha\gamma}(|\mathbf{r}_\alpha^{(i)}-\mathbf{r}_\gamma^{(j)}|)+\sum_{\alpha,i}U_{\mathrm{core}}(\mathbf{r}_\alpha^{(i)})\\ &\quad+\Delta\mathcal{W}_{\mathrm{sf}}(\mathbf{R}_1,\mathbf{R}_2,\ldots)+\Delta\mathcal{W}_{\mathrm{rf}}(\mathbf{R}_1,\mathbf{R}_2,\ldots),\end{aligned} \tag{6}$$

where $u_{\alpha\gamma}$ is the direct ion–ion interaction, U_{core} is a repulsive potential preventing core–core overlap of the ions with the channel and membrane, $\Delta\mathcal{W}_{\mathrm{sf}}$ is the shielded static external field coming from the permanent protein charge distribution and the transmembrane potential, and $\Delta\mathcal{W}_{\mathrm{rf}}$ is the reaction field arising from the electrostatic polarization of the various dielectric boundaries and the implicit salt in the outer region. We now describe each term contributing to $\mathcal{W}$ in detail.

The direct interaction between two ions separated by a distance r in the bulk solution is

$$u_{\alpha\gamma}(r)=4\epsilon_{\alpha\gamma}\left[\left(\frac{\sigma_{\alpha\gamma}}{r}\right)^{12}-\left(\frac{\sigma_{\alpha\gamma}}{r}\right)^{6}\right]+\frac{q_\alpha q_\gamma}{\epsilon_{\mathrm{bulk}}r}, \tag{7}$$

where $\epsilon_{\alpha\gamma}$ and $\sigma_{\alpha\gamma}$ are the parameters of the Lennard-Jones 6-12 (LJ) potential, q_α and q_γ are the charge of the ions, and ϵ_{bulk} is the dielectric constant of bulk water. Equation (7) corresponds to the well-known restricted primitive model with soft core which has been frequently used in statistical mechanical studies of ionic solutions.[11–13,27] The contribution from the static field is

$$\Delta\mathcal{W}_{\mathrm{sf}}(\mathbf{R}_1,\mathbf{R}_2,\ldots)=\sum_{\alpha,i}q_\alpha\,\phi_{\mathrm{sf}}(\mathbf{r}_\alpha^{(i)}), \tag{8}$$

where the electrostatic potential $\phi_{\mathrm{sf}}(\mathbf{r}_\alpha^{(i)})$ is calculated with the modified PB equation.[14,28]

Simulation region, side I and II :

$$\nabla\cdot[\epsilon(\mathbf{r})\nabla\phi_{\mathrm{sf}}(\mathbf{r})]=-4\pi\rho_p(\mathbf{r}).$$

Outer region, side I :

$$\nabla\cdot[\epsilon(\mathbf{r})\nabla\phi_{\mathrm{sf}}(\mathbf{r})]-\bar{\kappa}^2(\mathbf{r})[\phi_{\mathrm{sf}}(\mathbf{r})]=-4\pi\rho_p(\mathbf{r}). \tag{9}$$

Outer region, side II :

$$\nabla\cdot[\epsilon(\mathbf{r})\nabla\phi_{\mathrm{sf}}(\mathbf{r})]-\bar{\kappa}^2(\mathbf{r})[\phi_{\mathrm{sf}}(\mathbf{r})-V_{\mathrm{mp}}]=-4\pi\rho_p(\mathbf{r}),$$

where $\epsilon(\mathbf{r})$ and $\bar{\kappa}^2(\mathbf{r})$ are the space-dependent dielectric constant and Debye–Hückel screening factor and $\rho_p(\mathbf{r})$ is the charge density of the channel protein. It should be noted that there is no screening factor $\bar{\kappa}^2(\mathbf{r})$ in Eq. (9) for the PB equation corresponding to the regions where the ions are represented explicitly. The electrostatic fields arising from the protein charges and the potential difference across the membrane could be calculated separately by setting $V_{\mathrm{mp}}=0$ or $\rho_p(\mathbf{r})=0$ in Eq. (9), respectively. By virtue of the linearity of Eq. (9), they are simply superimposed in $\phi_{\mathrm{sf}}(\mathbf{r})$.[28] The contribution from the reaction field is

$$\Delta\mathcal{W}_{\mathrm{rf}}(\mathbf{R}_1,\mathbf{R}_2,\ldots)=\frac{1}{2}\sum_{\alpha,i}q_\alpha\,\phi_{\mathrm{rf}}(\mathbf{r}_\alpha^{(i)}), \tag{10}$$

where $\phi_{\mathrm{rf}}(\mathbf{r}_\alpha^{(i)})$ is the reaction field potential at $\mathbf{r}_\alpha^{(i)}$. The reaction field potential is defined as $\phi_{\mathrm{rf}}(\mathbf{r})=[\phi_s(\mathbf{r})-\phi_{\mathrm{bulk}}(\mathbf{r})]$, where $\phi_s(\mathbf{r})$ is the electrostatic potential computed for the complex solvent-channel environment, and $\phi_{\mathrm{bulk}}(\mathbf{r})$ is the electrostatic potential computed for a reference system corresponding to a uniform bulk solvent at zero salt concentration. The potential for the reference system is calculated from the Poisson equation

$$\epsilon_{\mathrm{bulk}}\nabla^2\phi_{\mathrm{bulk}}(\mathbf{r})=-4\pi\rho_{\mathrm{ion}}(\mathbf{r}), \tag{11}$$

and the potential for the complex solvent-channel dielectric environment is calculated from the PB equation

$$\nabla\cdot[\epsilon(\mathbf{r})\nabla\phi_s(\mathbf{r})]-\bar{\kappa}^2(\mathbf{r})\phi_s(\mathbf{r})=-4\pi\rho_{\mathrm{ion}}(\mathbf{r}), \tag{12}$$

where $\rho_{\mathrm{ion}}(\mathbf{r})$ is the charge density of all the explicit ions in the system [i.e., $\rho_{\mathrm{ion}}(\mathbf{r})=\Sigma_{\alpha,i}q_\alpha\,\delta(\mathbf{r}-\mathbf{r}_\alpha^{(i)})$]. Fixed protein charges and the transmembrane potential do not appear in Eq. (12) because their influence is already incorporated into the static field contribution. The ionic screening factor $\bar{\kappa}^2(\mathbf{r})$ in Eq. (12) is set to its bulk value in the outer region, where ions are treated implicitly, but is set to zero in the buffer and inner regions, where ions are simulated explicitly. It should be noted that the present treatment of the reaction field implies that the dielectric constant inside the ion is the same as that of the surrounding bulk solvent, i.e., the spatial dependence of the dielectric function is not affected by the displacement of the ions. The ions are thus treated as point charges in Eqs. (11) and (12). The influence of the finite size of the ions on the reaction field is relatively small and can be neglected.[29] However, because the transfer of a point charge

across a dielectric interface would yield an infinite self energy, the ions must remain within the dielectric solvent region.

One cycle of GCMC/BD corresponds to one step of BD followed by a few steps of GCMC (typically 5 or 10) to maintain the buffer regions in equilibrium. The evaluation of the forces acting on the ions is thus required at every dynamical time step of the stochastic trajectory. Because neither $\epsilon(\mathbf{r})$ nor $\overline{\kappa^2}(\mathbf{r})$ depends on the instantaneous configuration of the explicit ions in the system, Eq. (9) can be solved once using standard finite-difference methods and the result tabulated for efficient computer simulations.[30–32] The forces (first derivative of the potential) are then calculated analytically from the grid-based potential.[9,33] In contrast, it is not useful to tabulate $\phi_{\mathrm{rf}}(\mathbf{r})$ since it depends on the instantaneous position of all the ions in the simulation region. In order to incorporate the influence of the reaction field while avoiding the repeated calculation of the reaction field by solving the PB equation at every dynamical time step it is necessary to design an efficient method. This is described in the following section.

B. Basis-set expansion for the reaction field

The contribution of the reaction field to the multi-ion PMF can also be expressed as

$$\Delta\mathcal{W}_{\mathrm{rf}}(\mathbf{R}_1,\mathbf{R}_2,\ldots) = \frac{1}{2}\int d\mathbf{r}\,d\mathbf{r}'\;\rho_{\mathrm{ion}}(\mathbf{r})G_{\mathrm{RF}}(\mathbf{r},\mathbf{r}')\rho_{\mathrm{ion}}(\mathbf{r}'), \tag{13}$$

where $G_{\mathrm{RF}}(\mathbf{r},\mathbf{r}')$ is the Green's function corresponding to the reaction field potential at $\mathbf{r}$ arising from a point charge located at $\mathbf{r}'$. $G_{\mathrm{RF}}(\mathbf{r},\mathbf{r}')$ could, in principle, be stored but, it is a function of six independent Cartesian coordinates and this would require excessive memory resources and computations. To reduce these requirements, Chung and co-workers assumed an azimuthal symmetry of the dielectric boundary and store the reaction field Green's function in a five-dimensional table.[6,7,10,17] These difficulties are circumvented by expressing the ion charge distribution in the simulation region using a normalized basis set $\{b_m(\mathbf{r})\}$ with N basis functions,

$$\rho_{\mathrm{ion}}(\mathbf{r}) = \sum_m^N c_m\, b_m(\mathbf{r}). \tag{14}$$

The coefficients c_m can be written as

$$c_m = \sum_n S_{mn}^{-1}\, Q_n, \tag{15}$$

where the elements of the overlap matrix $\mathbf{S}$ and the generalized multipole moment vector $\mathbf{Q}$ are given by

$$S_{nm} = \int d\mathbf{r}\, b_n(\mathbf{r}) b_m(\mathbf{r}), \tag{16}$$

$$Q_n = \sum_{\alpha\, i} q_\alpha\, b_n(\mathbf{r}_\alpha^{(i)}). \tag{17}$$

In general, the basis functions generated for irregular geometries do not form an orthonormal set. In terms of Eqs. (13)–(15), the basis-set representation on $\Delta\mathcal{W}_{\mathrm{rf}}$ becomes

$$\begin{aligned}\Delta\mathcal{W}_{\mathrm{rf}} &= \frac{1}{2}\int d\mathbf{r}\,d\mathbf{r}'\left[\sum_{im}^N S_{im}^{-1}\,Q_m\,b_i(\mathbf{r})\right]G_{\mathrm{RF}}(\mathbf{r},\mathbf{r}')\\ &\quad\times\left[\sum_{jn}^N S_{jn}^{-1}\,Q_n\,b_j(\mathbf{r}')\right]\\ &= \frac{1}{2}\sum_{mn}^N\sum_{ij}^N S_{im}^{-1}\,Q_m\\ &\quad\times\left[\int d\mathbf{r}\,d\mathbf{r}'\;b_i(\mathbf{r})G_{\mathrm{RF}}(\mathbf{r},\mathbf{r}')b_j(\mathbf{r}')\right]S_{jn}^{-1}\,Q_n\\ &= \frac{1}{2}\sum_{mn}^N Q_m\left[\sum_{ij}^N S_{im}^{-1}\,M_{ij}S_{jn}^{-1}\right]Q_n\\ &= \frac{1}{2}\sum_{mn}^N Q_m\,M_{mn}^*\,Q_n. \end{aligned}\tag{18}$$

$\mathbf{M}^*$ is a constant matrix for the system which represents the reaction field Green's function between the generated multipolar basis functions (multipoles). $\mathbf{M}^*$ is equivalent to $\mathbf{M}$ if the basis set is made up of orthonormal functions, i.e., $S_{nm}=\delta_{nm}$. Although the generalized multipole moments Q_n are calculated for each instantaneous ion configuration during BD simulations, it should be noted that $\mathbf{M}^*$ does not depend on the instantaneous configuration because $\epsilon(\mathbf{r})$ and $\overline{\kappa^2}(\mathbf{r})$ are assumed to be independent of the ion configuration. Therefore, $\mathbf{M}^*$ is calculated once and stored for efficient BD simulations. The reaction field contribution to the total force acting on an ion of type α is

$$\mathbf{F}_\alpha^{(i)} = -q_\alpha\sum_{mn}^N Q_m\,M_{mn}^*\left(\frac{\partial b_n(\mathbf{r})}{\partial\mathbf{r}}\right)_{\mathbf{r}=\mathbf{r}_\alpha^{(i)}}. \tag{19}$$

C. Generation of basis-set functions and calculation of reaction field matrix

The following procedure is used to construct the basis set $\{b_m(\mathbf{r})\}$ for supporting the ion charge density ρ_{ion} in the calculation of the reaction field matrix $\mathbf{M}^*$. A complete basis set $\{f_m(\mathbf{r})\}$ formed by standard analytical functions is chosen. Spherical harmonics or Legendre polynomials are particularly convenient because of their simplicity, but other functions could be used (e.g., plane waves). The basis functions $b_m(\mathbf{r})$ are then generated with a shape function $\mathcal{S}(\mathbf{r})$ which is equal to one in all ion-accessible regions and zero otherwise (see Fig. 1),

$$b_m(\mathbf{r}) \equiv \mathcal{S}(\mathbf{r}) f_m(\mathbf{r}). \tag{20}$$

The resulting basis functions are nonzero only in the ion-accessible space of the simulation region but zero in the core and vicinity of the protein and membrane. This prescription is necessary to avoid any transfer of charge across dielectric

interfaces which would yield an infinite self-energy. Because of this operation, the basis set is no longer constituted of normalized orthogonal functions.

Having generated an appropriate basis set $\{b_m(\mathbf{r})\}$ for the simulation region the matrix $\mathbf{M}$ is calculated by exploiting the fact that the nmth matrix element corresponds to the interaction between the reaction field due to the charge density supported by the basis function $b_m(\mathbf{r})$ and the charge density of $b_n(\mathbf{r})$,

$$\mathrm{M}_{nm} = \int d\mathbf{r}\, d\mathbf{r}'\; b_n(\mathbf{r}) G_{\mathrm{RF}}(\mathbf{r},\mathbf{r}') b_m(\mathbf{r}') = \int d\mathbf{r} b_n(\mathbf{r}) \phi_{\mathrm{rf}}(\mathbf{r}; b_m(\mathbf{r})), \tag{21}$$

where $\phi_{\mathrm{rf}}(\mathbf{r};b_m(\mathbf{r})) \equiv [\phi_s(\mathbf{r};b_m(\mathbf{r})) - \phi_{\mathrm{bulk}}(\mathbf{r};b_m(\mathbf{r}))]$ is the reaction field due to the basis function $b_m(\mathbf{r})$. After turning off all protein charges in the system, the PB equation is solved with the complex solvent-channel environment using the basis function,

$$\nabla\cdot[\epsilon(\mathbf{r})\nabla\phi_s(\mathbf{r};b_m(\mathbf{r}))] - \overline{\kappa^2}(\mathbf{r})\phi_s(\mathbf{r};b_m(\mathbf{r})) = -4\pi b_m(\mathbf{r}). \tag{22}$$

In Eq. (22), the screening factor $\overline{\kappa^2}(\mathbf{r})$ is set to zero in the simulation region where ions are explicitly simulated. The reaction field is then calculated by subtracting the electrostatic potential from the reference primitive model,

$$\epsilon_{\mathrm{bulk}}\nabla^2\phi_{\mathrm{bulk}}(\mathbf{r};b_m(\mathbf{r})) = -4\pi b_m(\mathbf{r}). \tag{23}$$

These steps are repeated for N basis functions. The matrix elements are calculated by projecting the reaction field of the basis function b_m onto a charge distribution corresponding purely to the basis function b_n and calculating the integral Eq. (21) for $n=1,\ldots,N$.

Numerical problems in the evaluation of $\mathbf{M}^*$ are encountered in calculating the inverse of the matrix $\mathbf{S}$, even though the theoretical formulation of Eq. (18) is rigorous and general. Such problems are caused by the near linear dependence introduced by Eq. (20) in the basis set.[34] In order to circumvent the numerical problem the vector $\mathbf{C}$ in Eq. (15) can be practically formulated.

$$\mathbf{C} = \mathbf{X}\mathbf{X}^{\mathrm{T}}\mathbf{Q}, \tag{24}$$

where the matrix $\mathbf{X}$ is defined as $\mathbf{X} = \mathbf{S}^{-1/2}\mathbf{U}$. It is clear that Eq. (24) is equivalent to Eq. (15) if the matrix $\mathbf{U}$ is a unitary matrix, i.e., $\mathbf{U}^{\mathrm{T}}\mathbf{U} = \mathbf{1}$. Using a unitary transformation, i.e., $\mathbf{U}^{\mathrm{T}}\mathbf{S}\mathbf{U} = \mathbf{s}$, the matrix $\mathbf{X}$ can be rewritten as

$$\mathbf{X} = \mathbf{U}\mathbf{s}^{-1/2}, \tag{25}$$

where $\mathbf{s}$ is a diagonal matrix of the eigenvalues of $\mathbf{S}$. (In fact, the matrix $\mathbf{X}$ corresponds to a transformation matrix which transforms a nonorthogonal basis set to an orthogonal set.[34]) It is clear that the numerical problem arises from the singularity in $\mathbf{S^{-1}}$ for zero or near zero eigenvalues. The problem can be circumvented by sorting the eigenvalues and discarding the eigenvalues below a predefined cutoff eigenvalue $s_{\min}$ (see Sec. III). Assuming that the last M columns of $\mathbf{X}$ are eliminated to give a truncated $N\times(N-M)$ matrix $\tilde{\mathbf{X}}$, the coefficients c_m become

$$c_m = \sum_n^N X^*_{mn} Q_n, \tag{26}$$

where X^*_{mn} are given by

$$X^*_{mn} = \sum_k^{N-M} \tilde{X}_{mk}\tilde{X}_{nk}. \tag{27}$$

Using Eq. (26) instead of Eq. (15), the matrix $\mathbf{M}^*$ is then given by

$$M^*_{mn} = \sum_{ij}^N X^*_{im} M_{ij} X^*_{jn}. \tag{28}$$

Therefore, using a predefined cutoff eigenvalue $s_{\min}$ to truncate the matrix $\mathbf{X}$ in Eq. (25), $\mathbf{X}^*$ in Eq. (27) and $\mathbf{M}^*$ in Eq. (28) can be calculated for reaction field calculations without numerical problems. The generalized basis-set expansion method has been implemented into the PBEQ/GSBP module[16,20,28,33,35] of biomolecular simulation program CHARMM.[36]

TABLE I. Ion parameters.

Ion	ϵ^a (kcal/mol)	σ^a (Å)	D^b (Å^2/ps)	$\Delta\mu^c$ (kcal/mol) 1.0 M KCl	$\Delta\mu^c$ (kcal/mol) 0.2 M KCl
K^+	0.0870	3.142 645	0.196	−0.309 08	−0.205 91
Cl^-	0.1500	4.044 680	0.203	−0.333 63	−0.210 11

[a]Taken from Ref. 44.
[b]Taken from Ref. 45.
[c]Taken from Ref. 9.

III. NUMERICAL TESTS AND APPLICATIONS

The generalized basis-set expansion method is first tested and illustrated with three simple models. The method is then applied to a realistic atomic model of the cation-selective matrixporin (OmpF) from the outer membrane of *Escherichia coli* (*E coli*).[37] A spherical simulation region is taken into account for the simple models while an orthorhombic simulation region is used for the OmpF channel. Ion parameters are given in Table I. All the calculations were performed on a single Pentium III 600 MHz processor.

A. Tests on simple models

In the following the method is first tested and illustrated with three simple simulation systems: a uniform isotropic ionic salt solution, a salt solution in the presence of an impermeable membrane, and a salt solution in the presence of an impermeable membrane with a cylindrical pore. Unless specified explicitly, the following computational scheme was used for all three simple models. The radius of the spherical simulation region centered at the origin was 25 Å. All PB calculations were performed using a 75^3 grid with a grid spacing of 1.5 Å followed by a 115^3 grid with a grid spacing of 0.5 Å. Both grids (coarse and fine) were centered at the

origin. The dielectric constants of bulk water and membrane, ϵ_{bulk} and ϵ_{m}, were 80 and 2, respectively, and the concentration of implicit salt in the outer region was 1 M. To define the ion-accessible region, an ion exclusion Stern layer was set to 1.8 Å, which is the average radius of K^+ and Cl^- ions. Two basis sets were generated for the reaction field matrix $\mathbf{M}^*$. The first set was made up of a total of 361 basis functions of 19 multipoles ($L=18$) based on spherical harmonics. The second set constituted a total of 343 basis functions of the first 7 Cartesian Legendre polynomials in each direction. Legendre polynomials support multipolar charge distributions in a cube defined by -25 Å$<X,Y,Z<25$ Å. Its contribution outside the spherical simulation region was set to zero. The cutoff eigenvalue $s_{\min}$ in Eq. (25) was determined empirically using finite-difference PB calculations as a reference.

1. Influence of implicit salt in the outer region (test1)

The GCMC/BD simulation algorithm considers explicitly only the ions within a finite simulation region (see Fig. 1). Within this framework, the influence of the counterions located in the outer region is incorporated implicitly via the reaction field. As an illustration, we consider a spherical simulation system of 25 Å radius. Since the reference state is the pure solvent (ϵ_{bulk} everywhere), the reaction field energy corresponding to the electrostatic charging free energy of the charge distribution inside a spherical region embedded in a 1 M KCl salt solution is expressed in closed form by the Kirkwood multipolar expansion,[38]

$$\Delta \mathcal{W}_{\text{rf}}(\bar{\kappa}) = -\frac{4\pi|Q_{00}|^2}{2\epsilon_{\text{bulk}}}\frac{\bar{\kappa}}{(1+\bar{\kappa}a)} - \frac{4\pi\bar{\kappa}^2}{2\epsilon_{\text{bulk}}} \times \sum_{l=1}^{L}\sum_{m=-l}^{l}\frac{|Q_{lm}|^2}{(2l-1)(2l+1)^2}\frac{1}{a^{2l-1}}\frac{K_{l-1}(\bar{\kappa}a)}{K_{l+1}(\bar{\kappa}a)}, \tag{29}$$

where $a=25$, $L=18$ (19 multipoles), $\bar{\kappa}=0.32$ Å^{-1} (1 M salt concentration), and the polynomials $K_n(x)$ and the multipole moment Q_{lm} are given by

$$K_n(x) = \sum_{s=0}^{n}\frac{2^s n!(2n-s)!}{s!(2n)!(n-s)!}x^s, \tag{30}$$

$$Q_{lm} = \sum_{\alpha} q_\alpha Y_{lm}(\theta_\alpha,\phi_\alpha)|\mathbf{r}_\alpha|^l, \tag{31}$$

where α is an index for point charges and Y_{lm} is the spherical harmonics.[20,39] The accuracy of the basis-set expansion can be examined by comparing with the analytical results from Eq. (29) and with finite-difference numerical PB calculations.

The spherical multipolar functions constitute an orthogonal basis set in the spherical system, whereas Legendre polynomials do not because they are set to zero in the outer region (see Fig. 1). The linear dependence between the basis functions generated with Eq. (20) using Legendre polynomials can be eliminated by determining a cutoff eigenvalue $s_{\min}$ in order to truncate $\mathbf{X}$ in Eq. (25). For this purpose, 50 random configurations of K^+ and Cl^- ions were generated by GCMC simulations of 1 M KCl without reaction field. Each configuration has around a total of 70 ions. Reaction field energies using the generated basis functions were calculated as a function of $s_{\min}$. $s_{\min}=0.0005$ showed a best fit to PB results with an average energy error of 0.49 kcal/mol. In case of spherical harmonics, the average energy error was 0.19 kcal/mol with $s_{\min}=0.0$. Figure 2 shows the reaction field energies of 50 configurations calculated from Kirkwood's Eq. (29), PB, the basis-set expansions using spherical harmonics and Legendre polynomials. In this simple model, the reaction field energies are all negative because the interaction with the implicit salt outside the system is always favorable. The generalized basis-set expansion shows an excellent agreement with the results from finite-difference PB or Kirkwood's Eq. (29). In particular, the basis-set expansion with spherical harmonics and Kirkwood's Eq. (29) are almost identical even though the latter is an analytical multipolar expansion and the former uses a matrix $\mathbf{M}_{ij}$ that was obtained from finite-difference PB calculations with a discretized grid. Concerning the computational efficiency, it should be noted that PB calculations for 50 random configurations took around 4 h whereas the basis-set expansion took only 1 s of CPU time (with spherical harmonics or Legendre polynomials).

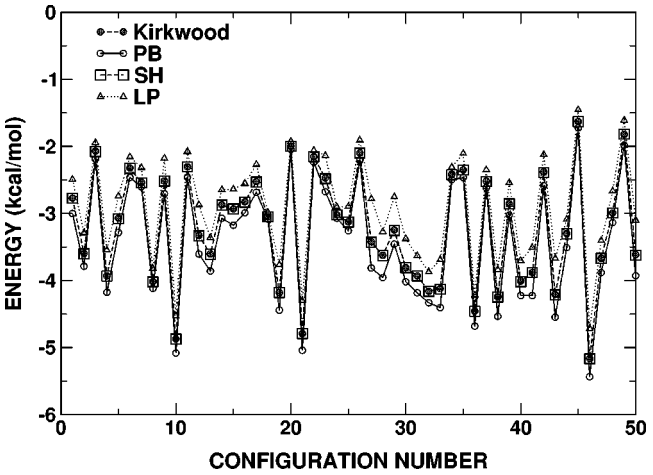

FIG. 2. Reaction field energies for 50 random configurations in the case of a 1 M KCl salt solution simulated inside a spherical region. The results from Kirkwood's multipolar expansion Eq. (29), finite-difference PB, and basis-set expansion based on spherical harmonics (SH) and Legendre polynomials (LP) are shown.

To illustrate the influence of the reaction field on the equilibrium structure of a simple ionic solution, we have performed GCMC/BD simulations of a 1 M KCl solution, with and without reaction field. The entire simulation system was treated as a GCMC buffer region (i.e., we allowed particles to be created or destroyed everywhere in the system). After some equilibration, GCMC/BD simulations of 25 ns were generated with a time step of 25 fs; 10 steps of GCMC were performed for each step of BD. Figure 3 shows the radial distribution functions of the K^+ ion density relative to the center of the simulation system (the distribution of Cl^- is almost identical and not shown here for the sake of clarity). As expected, one effect of the reaction field (arising from the implicit salt outside the simulation region) is to increase the

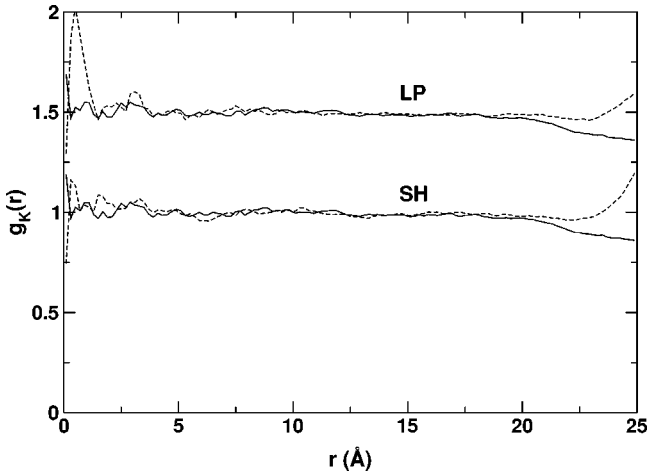

FIG. 3. Distribution of the K^+ relative to the center of a spherical simulation system for a 1 M KCl salt solution. The results obtained without reaction field (solid lines), and with reaction field (dashed lines) incorporated using a basis-set expansion based spherical harmonics (SH) and Legendre polynomials (LP) are shown. For clarity, the distribution function obtained with LP has been shifted vertically by 0.5. A perfectly uniform system should have a radial distribution equal to unity throughout the entire simulation region (note: the observed deviations at small distance r are due to poor sampling in the small volume).

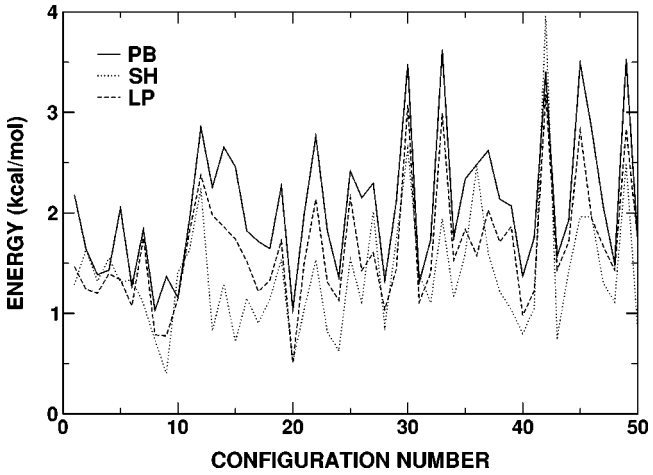

FIG. 4. Reaction field energies for 50 random configurations of ions near an impermeable planar membrane. The results from finite-difference PB and the basis-set expansion with spherical harmonics (SH) and Legendre polynomials (LP) are shown.

ion density near the edge of the simulation system. However, it appears to be slightly overestimated. This is probably caused by the neglect of other contributions, such as ion packing and core–core repulsion, in the multi-ion PMF Eq. (6). The influence of such nonpolar short-range contributions becomes increasingly important at high concentration, but are negligible under physiological conditions (around 150 mM salt). In addition, the basis-set expansion becomes less accurate when the ion get too close to the (implicit salt) boundary. This problem, which is also well known in applications of the Kirkwood multipolar expansion,[20,38] arises because the expansion is truncated to a finite number of basis functions. Nonetheless, including the reaction field is necessary for the correct equilibrium structure. The expected number of ions in the system is 39.4 for both K^+ and Cl^-, while the average numbers of K^+ and Cl^- are 37.3 and 37.3 (without reaction field), 39.5 and 39.3 (basis-set expansion based on spherical harmonics), and 39.2 and 39.0 (basis-set expansion based on Legendre polynomials), respectively.

2. Influence of image charges at the dielectric boundary (test2)

An important aspect of the reaction fields arising from the dielectric boundaries in the system is manifested as a repulsive force acting on the ions as they diffuse in the high dielectric bulk solution and approach a region with a low dielectric constant (membrane or protein). To test the ability of the basis-set expansion to reproduce this effect, we consider a spherical system of 25 Å radius with a low dielectric ion-impermeable membrane of 24 Å thickness centered at the origin. The ion-accessible region is thus restricted to the region outside the membrane plus the Stern layer of 1.8 Å ($|z|>13.8$ Å). In contrast to the previous illustration, a very low salt concentration, 0.001 M KCl, was considered intentionally so that the reaction field energy arises only from the induced surface (image) charges on the low-dielectric slab with $\epsilon_m=2$ because the reference state is the pure solvent (ϵ_{bulk} everywhere). Both basis functions generated from spherical harmonics and Legendre polynomials do not form orthogonal sets. Following the procedure described previously the optimal cutoff s_{min} was determined to be 0.005 for spherical harmonics and 0.002 for Cartesian Legendre polynomials. Average energy errors were 0.72 kcal/mol (spherical harmonics) and 0.42 kcal/mol (Legendre polynomials), respectively. Figure 4 shows the reaction field energies of 50 random configurations from PB and both basis-set expansions. In contrast to the previous test, the reaction field energies are now all positive because of the image charge repulsion. Despite a slight underestimation, the basis-set expansion is in a good agreement with finite-difference PB calculations.

Figure 5 shows the variations in the reaction field energy

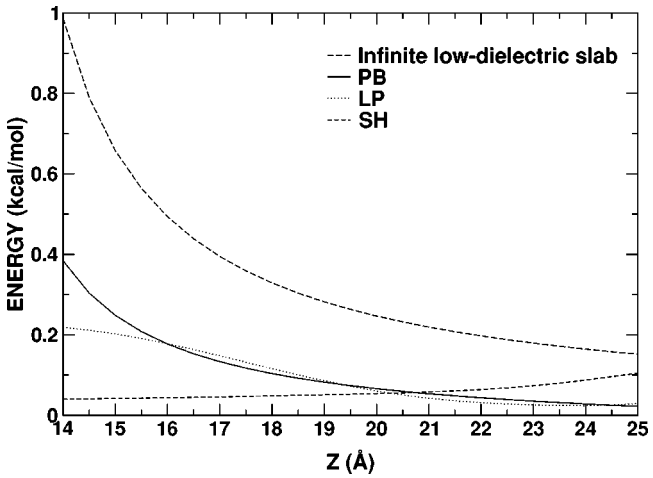

FIG. 5. Reaction field energies as a function of a moving point charge along the Z direction using Eq. (32) (infinite low-dielectric slab), finite-difference PB, and basis-set expansion based on spherical harmonics (SH) and Legendre polynomials (LP).

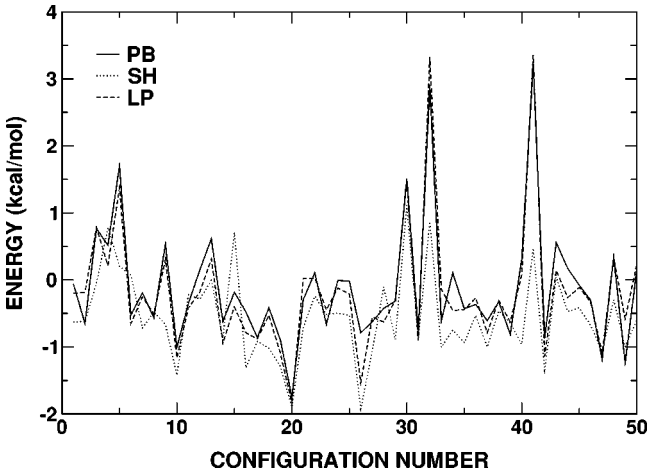

FIG. 6. Reaction field energies of 50 random configurations in a cylindrical pore system from PB and basis-set expansion based on spherical harmonics (SH) and Legendre polynomials (LP).

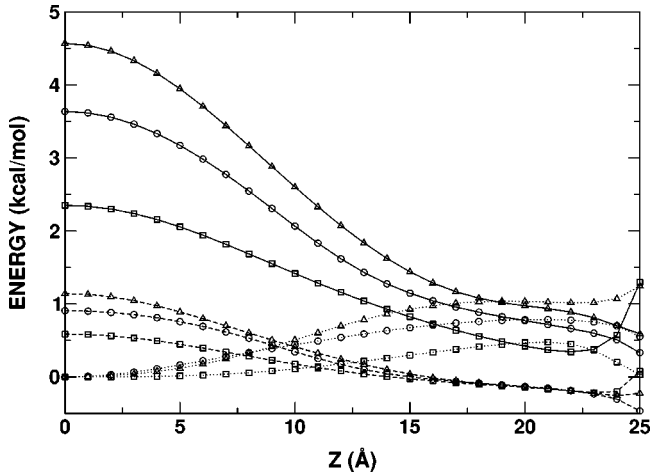

FIG. 7. Reaction field energies from PB (circle) and basis-set expansion based on spherical harmonics (square) and Legendre polynomials (triangle) as a function of a moving positive point charge (solid line) or a moving negative point charge (dotted line) along the Z direction when a positive point charge is centered at the origin. For comparison, the energies with a point charge (dashed line) along Z are also shown.

as a function of the position of a point charge along the Z direction. For a point ion q_α at z_α near an infinite dielectric interface located at z_{int}, the reaction field energy can be expressed as[39]

$$\Delta \mathcal{W}_{\text{rf}} = \frac{q_\alpha^2}{2\epsilon_{\text{bulk}}(z_\alpha - z_{\text{int}})} \frac{(\epsilon_{\text{bulk}} - \epsilon_m)}{(\epsilon_{\text{bulk}} + \epsilon_m)}. \tag{32}$$

In this simple case, the reaction field is equivalent to the interaction between the real charge q_α and a fictitious charge $q_\alpha(\epsilon_{\text{bulk}} - \epsilon_m)/(\epsilon_{\text{bulk}} + \epsilon_m)$ located symmetrically on the opposite side of the interface. For this reason, the reaction field is often referred to as ''image forces,'' in relation to the mathematical methods used to solve such problems in classical electrostatics.[39] Because the analytical expression [Eq. (32)] is often used to describe the reaction field acting on ions near a membrane, it is also of interest to examine the accuracy of this approximation in the case of a membrane of finite thickness. As shown in Fig. 5, the reaction field energy calculated numerically with finite-difference PB is approximately 60% of the value calculated with Eq. (32). The basis-set expansion based on Legendre polynomials reproduces PB calculations quite well except near the membrane, although the reaction field energy is quite low overall. In contrast to the previous illustration, as indicated in the energy errors and shown in Figs. 4 and 5, Legendre polynomials clearly generate a better basis function than spherical harmonics (see also the next example).

3. Aqueous cylindrical pore (test3)

Generally, there is an unfavorable energy barrier as ions move through a high dielectric pore surrounded by the low dielectric protein channel embedded in a membrane.[40] For meaningful GCMC/BD simulations of ion permeation, it is important to reproduce such unfavorable energy barrier with a reasonable accuracy. To test the basis-set expansion, we examined the energetics of ions along the axis of a simple cylindrical pore of 6 Å radius surrounded by a low dielectric ion-impermeable planar membrane of 24 Å thickness. Excluded in the Stern layer of 1.8 Å, ions can access both the cylindrical region with 4.2 Å radius and the bulk regions outside the membrane ($|z| > 13.8$ Å). Again, a spherical system of 25 Å radius is constructed. Using 50 random configurations as before, the optimal s_{min} was determined to be 0.0003 for spherical harmonics and 0.001 for Cartesian Legendre polynomials. Average energy errors were 0.56 kcal/mol (spherical harmonics) and 0.21 kcal/mol (Legendre polynomials), respectively. Figure 6 shows the reaction field energies of 50 configurations from PB and both basis sets. The basis-set expansion shows an excellent agreement with finite-difference PB calculations.

Figure 7 shows the variations in the reaction field energy as a function of the position of a moving (positive or negative) point charge when a positive point charge is fixed at the origin. For comparison, the reaction field energies of a point charge alone are also shown in Fig. 7. Because the reaction field arises from both the image charge in the dielectric boundary (see test2) and the implicit salt (1 M KCl) outside the system (see test1), the reaction field energy with a point charge varies from a positive number in the pore and near the membrane to a negative number near the system boundary. Since a positive point charge ($q_A = +1.0e$) is fixed at the origin, the total reaction field energy increases a lot as a positive charge q_B moves into the pore, whereas it decreases as a negative charge q_B moves into the pore. For example, PB calculations showed that the relative changes in the reaction field energy, which is defined as $\Delta\Delta\mathcal{W}_{\text{rf}} \equiv \Delta\mathcal{W}_{\text{rf}}(q_A, q_B) - \Delta\mathcal{W}_{\text{rf}}(q_A) - \Delta\mathcal{W}_{\text{rf}}(q_B)$, were 1.5 kcal/mol for $q_B = +1.0e$ and -1.5 kcal/mol for $q_B = -1.0e$ at $z_{q_B} = 5$ Å, respectively. This simple calculation shows that the ion pairing can form to reduce the unfavorable reaction field energy in narrow channels. The basis-set expansion based on Legendre polynomials shows an excellent agreement with PB calculations. It is clear that Legendre polynomials generate better basis functions than spherical harmonic does.

FIG. 8. The OmpF porin trimer viewed from the extracellular side [picture drawn with MOLSCRIPT (Ref. 46)].

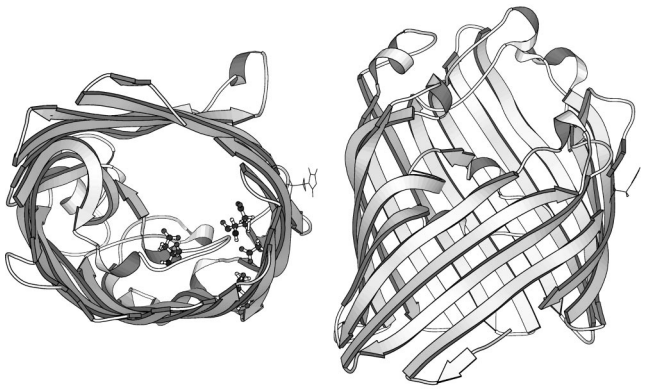

FIG. 9. One monomer of OmpF porin viewed from the top (left) and from the side (right) [picture drawn with MOLSCRIPT (Ref. 46)].

B. Application to a realistic atomic model of OmpF porin

So far, we have only used the generalized reaction field basis-set expansion method with simplified systems. As a final test and illustration, we now consider ion conduction through the aqueous channel of OmpF porin using a detailed atomic model of the protein bathed by a 200 mM KCl aqueous salt solution. OmpF is a well-characterized porin, both structurally and functionally, which makes it an excellent system for testing various ion permeation models.[41] Its three-dimensional structure has been determined to high resolution by x-ray crystallography.[37] OmpF folds into a trimeric structure (see Fig. 8), each monomer consisting of a 16-strand β barrel with short turns at the periplasmic side and large loops at the cell surface which confers a significant stability and rigidity to the structure. Each monomer possesses a wide aqueous pore (see Fig. 9), narrowed only to an elliptical cross section of around 7×11 Å by an internal loop called L3 at about half-way through the membrane, which suggests that the continuum electrostatics may be a valid approximation.

1. Computational details

An atomic system was constructed to perform GCMC/BD simulations with an orthorhombic region (44.5 Å$\times$44.5 Å$\times$86.5 Å) corresponding roughly to one OmpF monomer. Buffers of a 200 mM KCl salt solution were implemented from -37.75 to -35.5 Å and from $+46.5$ to $+48.75$ Å using the GCMC algorithm. The excess solvation energies are -0.206 and -0.210 kcal/mol for K^+ and Cl^-, respectively (see ion parameters in Table I). To setup the atomic system, the entire trimer with its symmetry axis oriented along the *Z* axis was embedded in an ion-impermeable planar membrane of 34 Å thickness. The default protonation state was used for all ionizable residues except for Glu296 and Asp312, which were protonated.[8,42] The net charge of the OmpF trimer is $-30e$. The atomic charges were taken from the all-atom PARAM22 force field[43] of the CHARMM program.[36]

The electrostatic potential (static field) arising from the protein charges was calculated with the modified PB Eq. (9) using a fully detailed atomic model of the OmpF trimer. For the nonequilibrium GCMC/BD simulations, the influence of the transmembrane potentials of $+100$ mV was included in the calculation of the electrostatic potential. A dielectric constant of 2 was used for the interior of the protein and membrane regions. A dielectric constant of 80 was assumed for the bulk solvent region including the aqueous pore region of OmpF. The optimized atomic radii for proteins were used to setup the dielectric boundary.[35] A Debye–Hückel screening factor $\overline{\kappa^2}$ corresponding to a 200 mM salt concentration was assigned only to the outer region. In addition to the protein atomic radii, an ion exclusion Stern layer of 1.8 Å corresponding to the average radius of K^+ and Cl^- was used to set the spatial dependence of the ionic screening factor. The electrostatic potential was first calculated with a coarse grid (101^3 points with a grid spacing of 1.5 Å) centered on the entire OmpF trimer with periodic boundary conditions imposed in the *X* and *Y* directions. The result of the coarse calculation was then used to set the potential on the edge of a smaller box to perform a second calculation using a finer grid ($101\times101\times181$ with a grid spacing of 0.5 Å) centered on the orthorhombic simulation region corresponding roughly to one OmpF monomer. The same computational procedure (with all protein charges turned off) was used to calculate the reaction field matrix $\mathbf{M}^*$ for a total of 225 basis functions generated from all combination of the 5, 5, and 9 Legendre polynomials in *X*, *Y*, and *Z* directions, respectively. All continuum electrostatic calculations were performed using the PBEQ/GSBP module[16,20,28,33,35] of CHARMM.[36]

The core repulsion potential map was calculated and stored on a grid which was set to one in all ion-accessible region and zero otherwise. The CHARMM PARM22 Lennard-Jones radii scaled by $2^{-1/6}$ and augmented by an ion exclusion Stern layer of 1.8 Å were used to setup the contact surface. The molecular surface including reentrant surface was then built to ensure that no region in the protein interior is accessible to the ions. For the sake of simplicity, a single

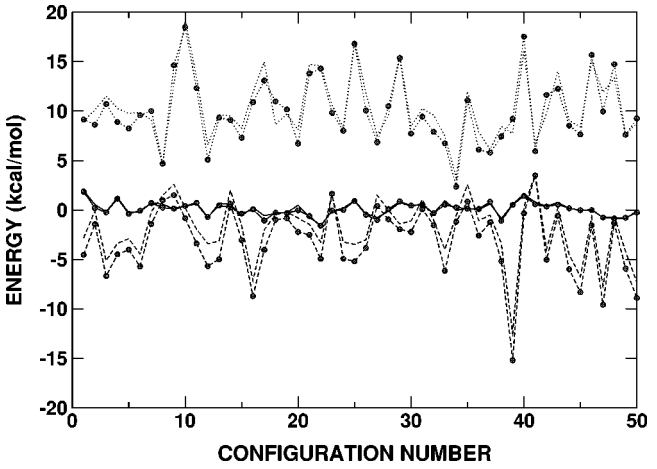

FIG. 10. Reaction field energies for 50 random configurations in OmpF from PB (closed circle) and basis-set expansion (no symbol) with different contributions to multi-ion PMF. The results when the configurations were generated with no static field and no reaction field (solid line), static field and no reaction field (dotted line), and static field and reaction field (dashed line) are shown.

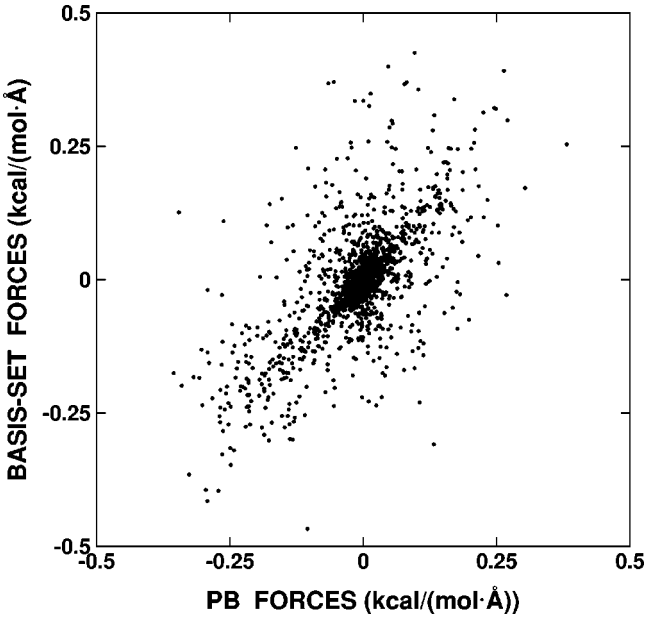

FIG. 11. Comparison of basis-set reaction field forces with the corresponding (exact) PB forces. A total of 691 ions in 25 random configurations in OmpF are considered. A few points (some components of 11 ions) were located outside the boundary of the plot. For the sake of clarity, the figure only shows the forces which are between -0.5 and 0.5 kcal/(mol Å).

uniform repulsive potential U_{core} of $+15$ kcal/mol was used for both ions. If needed, one could easily take into account the slight difference in size of K^+ and Cl^- by constructing and storing a repulsive potential map for each ion type. The GCMC/BD simulations were generated with a time step of 25 fs; 4 steps of GCMC were performed for each step of BD. The electrostatic energy and forces were calculated using a second-order B-spline (trilinear) interpolation and the repulsive energy and forces using a third-order B-spline interpolation.[9,33] The total length of each simulation was 1 μs. To obtain statistical convergence on the conductance in $V_{\text{mp}}=+100$ mV, 10 independent GCMC/BC simulations were generated with both different initial configuration and different seed numbers for the random number generator. A GCMC/BD simulation without the reaction field took about 7 h of CPU time while a GCMC/BD simulation with the reaction field took about 52 h.

The optimal cutoff eigenvalue s_{min} in Eq. (25) was determined to be 0.003 by comparing the basis-set results with finite-difference PB calculations for three different sets of 50 random configurations. Each configuration has around a total of 22 ions. The first set was generated with no static field and no reaction field, the second set with static field and no reaction field, and the last set with static field and reaction field. With this optimized cutoff, the average error between PB and basis-set reaction field energies were 0.14 ± 0.01 (first set), 0.98 ± 0.33 (second set), and 1.25 ± 0.30 (third set), respectively. Figure 10 shows the energies from PB and basis-set calculations for 50 configurations in each set. In Fig. 11, all *X*, *Y*, and *Z* components of the basis-set reaction field forces of 691 ions in 25 configurations in the second set are compared with the corresponding PB forces.[33] The average error on the force is 0.039 ± 0.059 kcal/(mol Å). There is a significant disagreement for some ions when they get too close to the dielectric boundary or the system boundary (some force components for 11 ions were located outside the plot boundary shown in Fig. 11) (data not shown). Such discrepancy should not affect the ion permeation significantly because the pore of OmpF porin is quite far from the system boundary. Furthermore, the core repulsion potential repels the ions when they get too close to the dielectric boundary. Lastly, it should be stressed that the PB force calculations for 50 random configurations took nearly 6 h of CPU time whereas the basis-set expansion took only 0.3 s. The basis set expansion thus provides the computational efficiency needed for BD simulations.

2. Equilibrium ion distribution

A series of 1 μs GCMC/BD simulations were performed to investigate the influence of the static field and the reaction

TABLE II. Number of K^+ and Cl^- ions from GCMC/BD simulations of OmpF.

Contributions included in multi-ion PMF	N_{syst}		N_{pore}[a]		
	K^+	Cl^-	$\langle K^+\rangle$	$\langle Cl^-\rangle$	$\langle K^+\rangle/\langle Cl^-\rangle$
No protein charges and no reaction field	9.0 ± 3.4	8.9 ± 3.4	0.43	0.44	1.0
Protein charges and no reaction field	15.3 ± 3.7	10.0 ± 3.5	4.16	0.11	37.8
Protein charges and reaction field	16.3 ± 4.4	6.6 ± 3.4	1.73	0.14	12.4

[a]The pore region is defined as the boundaries of the β barrel (-16 Å$\geqslant Z\leqslant 16$ Å).

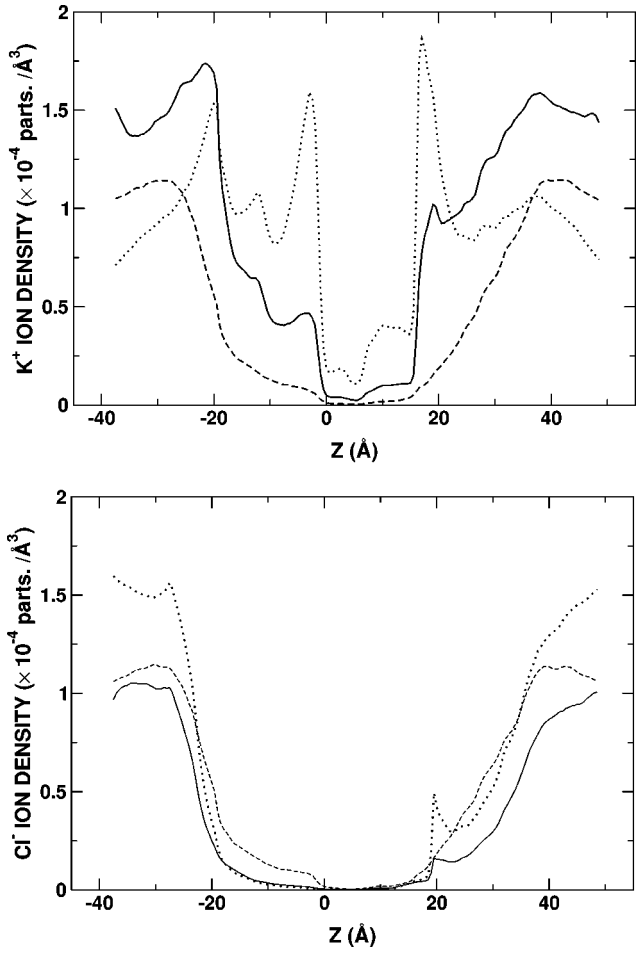

FIG. 12. Number density of K^+ and Cl^- ions from 1.0 μs GCMC/BD simulations with different contributions to multi-ion PMF; no static field and no reaction field (dashed line), static field and no reaction field (dotted line), and static field and reaction field (solid line).

field on the equilibrium ion distribution in OmpF. Both ion–ion interactions and hard-core repulsive potential energy were included in all simulations. The average number of K^+ and Cl^- ions in the system and in the pore are given in Table II. The pore region was defined as the part of the aqueous pore corresponding to the boundaries of the β barrel of OmpF. According to this definition, the OmpF channel pore nearly spans 32 Å from -16 to 16 Å along the Z axis. Figure 12 shows the ion density profiles in the system.

As expected, there is no difference in ion distributions when the static and reaction field are not included. It is observed in Fig. 12 that the densities of K^+ and Cl^- are lower than the expected value (1.2×10^{-4} part/Å^3) near the edge of the system. In analogy with the simulation of the simple salt solution (see test1), the neglect of the favorable interactions with the implicit salt outside the system gives rise to a local decrease in the density near the edges. Furthermore, a large number of K^+ ions occupy the interior of the pore when the static field arising from OmpF protein charges is included with no reaction field. Both dominant negative electrostatic potential and the absence of the unfavorable reaction field largely overestimate the K^+ density in the pore. This is the reason why all the reaction field energies shown in Fig. 10 are large positive numbers. The accumulation of K^+ ions in the pore results in a local increase of Cl^-, and a decrease of K^+ outside OmpF because of ion–ion interactions. When both reaction field and static field are included, as shown in Fig. 12, the K^+ density in the pore decreases dramatically. In analogy with the simple aqueous pore examined in test 3, this is caused by the unfavorable reaction field for an ion in a high dielectric pore surrounded by low dielectric protein. These calculations demonstrate that the reaction field in the multi-ion PMF plays an important role in the determination of ion densities in the channel.

3. Channel conductance

A series of 1 μs GCMC/BD simulations were performed to calculate the ionic current going through OmpF when a transmembrane potential of 100 mV is applied. The results of the simulations is summarized in Table III. With no static field and no reaction field, the current carried by Cl^- is slightly larger than the current carried by K^+ because of the difference in diffusion constants, i.e., $D_{K^+}/D_{Cl^-}=0.97$. There is a dramatic change in the cationic and anionic currents when the static field contribution from the protein charges is included in the PMF, making OmpF a cation-selective channel. As expected, the magnitude of the ionic current is reduced significantly when the unfavorable reaction field is included. The channel conductance changes from 1.0 to 0.42 nS when the reaction field is included. The latter value is in excellent accord with the conductance of 0.35 nS determined experimentally under the same conditions.[47] The quantitative agreement is remarkable given the simplicity of the present model.

IV. SUMMARY

A novel method has been developed to incorporate the electrostatic reaction field in BD simulations of ion diffusing through complex molecular pores of arbitrary geometry. The method has been implemented into the GCMC/BD algorithm introduced recently.[9] A multipolar basis-set expansion is used to express the reaction field Green's function matrix $\mathbf{M}^*$. The electrostatic energy and forces are calculated at each time step by updating the generalized multipole moments. The reaction field matrix, which provides the coupling be-

TABLE III. Ionic currents and conductance from GCMC/BD simulations of OmpF at +150 mV.

Contributions included in multi-ion PMF	I_{K^+} (pA)	I_{Cl^-} (pA)	$\langle I_{K^+}\rangle/\langle I_{Cl^-}\rangle$	G (nS)
No protein charges and no reaction field	10.2±1.3	10.8±1.2	0.95	0.21±0.02
Protein charges and no reaction field	98.3±3.5	1.7±0.7	57.91	1.00±0.03
Protein charges and reaction field	39.1±1.6	2.6±0.7	14.97	0.42±0.02

tween generalized multipoles, is calculated only once and stored before the BD simulations for computational efficiency.

Standard analytical functions such as spherical harmonics or Legendre polynomials were used to generate a general basis set allowing the treatment of arbitrary geometries. The inverse matrix needed for the nonorthonormal basis set can be regularized using a singular-value decomposition. It was shown that the results are accurate and the method computationally inexpensive for simple model systems and for a realistic atomic model of OmpF porin. From this point of view, the present advance represents an important extension to the GSBP method which was limited only to spherical and orthorhombic simulation regions.[19,20] It is possible that other standard functions could be used to generate the basis set such as plane waves, though Legendre polynomials appear to be remarkably convenient. In all the examples considered here, the results obtained with these simple and numerically inexpensive polynomials were more accurate than with spherical harmonics.

Importantly, the calculations show that an accurate treatment of the reaction field is needed for meaningful studies of ion conduction through OmpF porin. The calculated channel conductance is 1.0 nS when the reaction field is neglected, in poor agreement with the conductance of 0.35 nS determined experimentally under the same conditions.[47] However, when both the static and the reaction field are included, the calculated conductance is 0.42 nS, in excellent accord with the experimental value. This suggests that the reaction fields basis-set expansion with the GCMC/BD algorithm can be a useful approach for quantitative studies of ion conduction through complex molecular pores. Future work will examine ion selectivity and permeation through other porins using detailed atomic models.

ACKNOWLEDGMENTS

Useful discussions with Raimund Dutzler, Tilman Schirmer, and Nathalie Saint are gratefully acknowledged. This work was supported by a grant from NIH GM62342-01.

[1] K. Cooper, E. Jakobsson, and P. Wolynes, Prog. Biophys. Mol. Biol. **46**, 51 (1985).
[2] E. Jakobsson and S. Chiu, Biophys. J. **52**, 33 (1987).
[3] S. Chiu and E. Jakobsson, Biophys. J. **55**, 147 (1989).
[4] S. Bek and E. Jakobsson, Biophys. J. **66**, 1028 (1994).
[5] S. Li, M. Hoyles, S. Kuyucak, and S. Chung, Biophys. J. **74**, 37 (1998).
[6] S. Chung, M. Hoyles, T. Allen, and S. Kuyucak, Biophys. J. **75**, 793 (1998).
[7] S. Chung, T. Allen, M. Hoyles, and S. Kuyucak, Biophys. J. **77**, 2517 (1999).
[8] T. Schirmer and P. Phale, J. Mol. Biol. **294**, 1159 (1999).
[9] W. Im, S. Seefeld, and B. Roux, Biophys. J. **79**, 788 (2000).
[10] B. Corry, T. Allen, and S. K. S. Chung, Biophys. J. **80**, 195 (2001).
[11] D. Ermak, J. Chem. Phys. **62**, 4189 (1975).
[12] M. Wood and H. Friedman, Phys. Chem. Neue Folge **155**, 121 (1987).
[13] M. Jardat, O. Bernard, P. Turq, and G. Kneller, J. Chem. Phys. **110**, 7993 (1999).
[14] B. Roux, Biophys. J. **77**, 139 (1999).
[15] B. Roux and M. Karplus, J. Am. Chem. Soc. **115**, 3250 (1993).
[16] B. Roux, S. Bernèche, and W. Im, Biochemistry **39**, 13295 (2000).
[17] M. Hoyles, S. Kuyucak, and S. Chung, Phys. Rev. E **58**, 3654 (1998).
[18] P. Graf, A. Nitzan, M. Kurnikova, and R. Coalson, J. Phys. Chem. B **101**, 5239 (1997).
[19] B. Roux, D. Beglov, and W. Im, in *Proceedings of the Santa Fe Workshop on Treatment of Electrostatic Interactions in Computer Simulations of Condensed Media, 23-25 June 1999*, AIP Conf. Proc., edited by L. Pratt and G. Hummer **492**, 473 (1999).
[20] W. Im, S. Bernèche, and B. Roux, J. Chem. Phys. **114**, 2924 (2001).
[21] G. Heffelfinger and D. Ford, Mol. Phys. **94**, 659 (1998).
[22] A. Thompson, D. Ford, and G. Heffelfinger, J. Chem. Phys. **109**, 6406 (1998).
[23] P. Pohl and G. Heffelfinger, J. Membr. Sci. **155**, 1 (1999).
[24] A. Thompson and G. Heffelfinger, J. Chem. Phys. **110**, 10693 (1999).
[25] S. Chandrasekar, Rev. Mod. Phys. **15**, 1 (1943).
[26] W. McMillan and J. Mayer, J. Chem. Phys. **13**, 276 (1945).
[27] P. Ramanathan and H. Friedman, J. Chem. Phys. **54**, 1086 (1971).
[28] B. Roux, Biophys. J. **73**, 2980 (1997).
[29] B. Roux and R. MacKinnon, Science **285**, 100 (1999).
[30] J. Warwicker and H. Watson, J. Mol. Biol. **157**, 671 (1982).
[31] I. Klapper, R. Hagstrom, R. Fine, K. Sharp, and B. Honig, Proteins **1**, 47 (1986).
[32] A. Nicholls and B. Honig, J. Comput. Chem. **12**, 435 (1991).
[33] W. Im, D. Beglov, and B. Roux, Comput. Phys. Commun. **111**, 59 (1998).
[34] A. Szabo and N. Ostlund, *Modern Quantum Chemistry* (Dover, New York, 1996).
[35] M. Nina, D. Beglov, and B. Roux, J. Phys. Chem. B **101**, 5239 (1997).
[36] B. R. Brooks, R. E. Bruccoleri, B. D. Olafson, D. J. States, S. Swaminathan, and M. Karplus, J. Comput. Chem. **4**, 187 (1983).
[37] S. W. Cowan, T. Schirmer, G. Rummel, M. Steiert, R. Gosh, R. A. Pauptit, J. N. Jansonius, and J. P. Rosenbusch, Nature (London) **358**, 727 (1992).
[38] J. Kirkwood, J. Chem. Phys. **2**, 351 (1934).
[39] J. Jackson, *Classical Electrodynamics* (Wiley, New York, 1962).
[40] P. C. Jordan, Biophys. Chem. **13**, 20 (1981).
[41] T. Schirmer, J. Struct. Biol. **121**, 101 (1998).
[42] A. Karshikoff, A. Spassov, S. W. Cowan, R. Ladenstein, and T. Schirmer, J. Mol. Biol. **240**, 372 (1994).
[43] A. J. MacKerell, Jr., D. Bashford, M. Bellot *et al.*, J. Phys. Chem. B **102**, 3586 (1998).
[44] B. Roux, Biophys. J. **71**, 3177 (1996).
[45] B. Hille, *Ionic Channels of Excitable Membranes*, 2nd ed. (Sinauer, Sunderland, MA, 1992).
[46] P. Kraulis, J. Appl. Crystallogr. **24**, 946 (1991).
[47] N. Saint (private communication).